

Calculation of momentum correlation functions between π , K , and p for several heavy-ion collision systems at $\sqrt{s_{NN}} = 39$ GeV

Ting-Ting Wang (王婷婷) ^{1,2}, Yu-Gang Ma (马余刚) ^{1,3,*} and Song Zhang (张松) ^{1,3}

¹Key Laboratory of Nuclear Physics and Ion-Beam Application (MOE), Institute of Modern Physics, Fudan University, Shanghai 200433, China

²Shanghai Institute of Applied Physics, Chinese Academy of Sciences, Shanghai 201800, China

³Shanghai Research Center for Theoretical Nuclear Physics, NSFC and Fudan University, Shanghai 200438, China



(Received 1 October 2023; accepted 19 January 2024; published 15 February 2024)

Momentum correlation functions between π , K , and p are calculated for several heavy-ion collision systems, namely ${}^{10}_5\text{B} + {}^{10}_5\text{B}$, ${}^{16}_8\text{O} + {}^{16}_8\text{O}$, ${}^{40}_{20}\text{Ca} + {}^{40}_{20}\text{Ca}$, and ${}^{197}_{79}\text{Au} + {}^{197}_{79}\text{Au}$ in central collisions as well as ${}^{197}_{79}\text{Au} + {}^{197}_{79}\text{Au}$ collision in different centralities at center-of-mass energy $\sqrt{s_{NN}} = 39$ GeV within the framework of a multiphase transport model complemented by the Lednický and Lyuboshitz analytical method. The results present the centrality and system-size dependence of the momentum correlation functions among pairs of π , K , and p , from which the emission source-size can be deduced. It is found that the deduced source sizes increase with the decreasing of centrality for Au + Au system or with the increasing of system size in central collisions with different nuclear size. In addition, through the momentum correlation functions of nonidentical particle pairs gated on velocity, the average emission sequence of nonidentical particles can be indicated. The results illustrate that in the small relative momentum region, protons are emitted in average earlier than π^+ and K^+ , and K^+ are emitted averagely earlier than π^+ . Furthermore, it seems that larger interval of the average emission order among them is exhibited for smaller collision systems. The present study sheds light on the dynamics of light particle emission at RHIC energy.

DOI: [10.1103/PhysRevC.109.024912](https://doi.org/10.1103/PhysRevC.109.024912)

I. INTRODUCTION

In heavy-ion collisions (HICs), two-particle momentum correlation function, also called the Hanbury-Brown Twiss (HBT) interferometry, is different from the original application in astronomy [1,2], and has been normally utilized to extract space-time information of the emission source and probe the dynamical evolution of nuclear collisions in a wide energy range [3–12]. Many studies on the two-particle momentum correlation functions of different kinds of particles in HICs can be also found in literature [11,13–33], e.g., for mesons, neutrons, protons, light charged particles (LCP), and so on. Multivariable dependences, including centrality, system size, total momentum of particle pairs, isospin of the emission source, nuclear symmetry energy, nuclear equation of state (EOS), as well as in-medium nucleon-nucleon cross section (NNCS), etc., of different particle momentum correlation functions contain a wealth of information about the space-time characteristics of HICs. Even in antimatter zone,

the interaction between antiprotons has been measured with the momentum correlation functions and the charge-parity-time equality of interactions between $p - p$ and $\bar{p} - \bar{p}$ has been confirmed [34]. The momentum correlation functions for particles with strangeness have been also discussed, for instance Λ pairs [35], proton- Ω , and proton- Ξ , etc. [36,37]. Recently this method is extended to investigate the three-body interaction of hadrons in relativistic heavy-ion collisions [38]. Furthermore, theoretical study has been extended to different kinds of nonidentical particle pairs [11,15,29,30,39–44], from which information about emission sequence between pairs could be extracted as proposed in Ref. [45].

In this work we study the momentum correlation functions of like-sign and unlike-sign particles between π , K , and p in several ultrarelativistic heavy-ion collisions systems, namely ${}^{10}_5\text{B} + {}^{10}_5\text{B}$, ${}^{16}_8\text{O} + {}^{16}_8\text{O}$, ${}^{40}_{20}\text{Ca} + {}^{40}_{20}\text{Ca}$, and ${}^{197}_{79}\text{Au} + {}^{197}_{79}\text{Au}$ in central collisions as well as ${}^{197}_{79}\text{Au} + {}^{197}_{79}\text{Au}$ in different centralities at $\sqrt{s_{NN}} = 39$ GeV, which were simulated by a multiphase transport (AMPT) model [46,47]. The specific collision energy at 39 GeV was selected because it might be close to the critical point [48,49]. On the other hand, the small system physics was very interesting because the similar phenomena have been observed at high multiplicity events in p+p, p+Pb, d+Au collisions in comparison with Au + Au collision [50], and the system scan was motivated to probe the medium transport properties [51–54]. And ${}^{16}_8\text{O} + {}^{16}_8\text{O}$ collisions were conducted by STAR Collaboration [55] and will be performed by ALICE Collaboration [53]. Different gating

*Corresponding author: mayugang@fudan.edu.cn

Published by the American Physical Society under the terms of the [Creative Commons Attribution 4.0 International](https://creativecommons.org/licenses/by/4.0/) license. Further distribution of this work must maintain attribution to the author(s) and the published article's title, journal citation, and DOI. Funded by SCOAP³.

conditions such as centrality, system-size, total particle pair momentum (P_{tot}) as well as velocity of particle are applied to explore the momentum correlation functions of particle pairs, namely π , K , and p . In particular, we report on the indication of the emission chronology of the above mesons and baryon, which can be deduced from their corresponding momentum correlation functions gated with velocity of particles in HICs at $\sqrt{s_{NN}} = 39$ GeV.

The rest of this paper is organized as follows. In Sec. II A, we briefly describe a multiphase transport model [46,47], then introduce how to calculate the momentum correlation functions of particle pairs by using the Lednický and Lyuboshitz analytical formalism [3,56–59] in Sec. II B. In Sec. III, we summarize the simulated results of the particle momentum correlation functions gated on various parameters in different heavy-ion collisions. Section III A compares the results of like-sign and unlike-sign particle pairs momentum correlation functions with experimental data from the RHIC-STAR Collaboration. From Secs. III B–III D, identical and nonidentical particle momentum correlation functions gated on different conditions are systematically investigated and emission chronology of π , K , and p is discussed. Finally, a summary is given in Sec. IV.

II. MODELS AND FORMALISM

A. AMPT model

To obtain phase-space distributions of (anti)particles, a multiphase transport model [46,47] is used as an event generator, which has been applied successfully for studying heavy-ion collisions at relativistic energies [31,60–69]. In the version of melting AMPT, the initial phase-space information of partons is generated by the heavy-ion jet interaction generator (HIJING) model [70,71]. The interaction between partons is then simulated by Zhang’s parton cascade (ZPC) model [72]. During the hadronization process, a quark coalescence model is used to combine partons into hadrons [73–75]. Then, the hadronic rescattering evolution is described by a relativistic transport (ART) model [76].

The phase-space distributions of particles are selected at the final stage in the hadronic rescattering process (ART model [76]) with considering baryon-baryon, baryon-meson, and meson-meson elastic and inelastic scatterings, as well as resonance decay or weak decay.

B. Lednický and Lyuboshitz technique

AMPT model is not able to directly give the two-particle momentum correlation function because the quantum statistics (QS) effect and final-state interactions (FSI) [3,56] are not implemented in the model, therefore a momentum correlation function technique has to be introduced. One of the techniques of the two-particle momentum correlation function was proposed by Lednický and Lyuboshitz [57–59], which coupled with the phase-space from transport model or a simple Gaussian emission source to produce momentum correlation function. The method is based on the principle as follows: when two particles emitted at small relative momentum, their momentum correlation function is determined by the

space-time characteristics of the production processes owing to the effects of QS and FSI [3,56].

According to the conditions in Ref. [39], we obtain the following expression:

$$C(\mathbf{k}^*) = \frac{\int \mathbf{S}(\mathbf{r}^*, \mathbf{k}^*) |\Psi_{\mathbf{k}^*}(\mathbf{r}^*)|^2 d^4 \mathbf{r}^*}{\int \mathbf{S}(\mathbf{r}^*, \mathbf{k}^*) d^4 \mathbf{r}^*}, \quad (1)$$

where $\mathbf{r}^* = \mathbf{x}_1 - \mathbf{x}_2$ and $\mathbf{k}^* = \mathbf{q} = \frac{1}{2}(\mathbf{p}_1 - \mathbf{p}_2)$ are the relative distance and half of the relative momentum of the two particles in the pair rest frame (PRF) at their kinetic freezeout, respectively. $\mathbf{S}(\mathbf{r}^*, \mathbf{k}^*)$ is the probability to emit a particle pair with given \mathbf{r}^* and \mathbf{k}^* , i.e., the source emission function, and $\Psi_{\mathbf{k}^*}(\mathbf{r}^*)$ is the equal-time ($t^* = 0$) reduced Bethe-Salpeter amplitude, which can be approximated by the outer solution of the scattering problem in the PRF.

Momentum correlations of both identical and nonidentical particle pairs are influenced by the strong and Coulomb-induced correlations. In this calculation, for nonidentical charged pair, Coulomb interaction is dominant. Strong interaction is also present, but is expected to be small. The reduced Bethe-Salpeter amplitude can be approximated by the outer solution of the scattering problem. This is

$$\Psi_{\mathbf{k}^*}(\mathbf{r}^*) = e^{i\delta_c \sqrt{A_c(\lambda)}} \left[e^{-i\mathbf{k}^* \mathbf{r}^*} F(-i\lambda, 1, i\xi) + f_c(k^*) \frac{\tilde{G}(\rho, \lambda)}{r^*} \right], \quad (2)$$

where $\delta_c = \arg \Gamma(1 + i\lambda)$ is the Coulomb s -wave phase shift with $\lambda = (k^* a_c)^{-1}$. Here a_c is the two-particle Bohr radius, which is equal to 387 fm for pion-pion, and equal to 248.52, 222.56, and 83.59 fm for pion-kaon, pion-proton, and kaon-proton pairs. $A_c(\lambda) = 2\pi\lambda[\exp(2\pi\lambda) - 1]^{-1}$ is the Coulomb penetration factor, and its positive (negative) value corresponds to the repulsion (attraction). $\tilde{G}(\rho, \lambda) = \sqrt{A_c(\lambda)}[G_0(\rho, \lambda) + iF_0(\rho, \lambda)]$ is a combination of regular (F_0) and singular (G_0) s -wave Coulomb functions [58,59]. $F(-i\lambda, 1, i\xi) = 1 + (-i\lambda)(i\xi)/1!^2 + (-i\lambda)(-i\lambda + 1)(i\xi)^2/2!^2 + \dots$ is the confluent hypergeometric function with $\xi = \mathbf{k}^* \mathbf{r}^* + \rho$, $\rho = k^* r^*$.

$$f_c(k^*) = \left[K_c(k^*) - \frac{2}{a_c} h(\lambda) - ik^* A_c(\lambda) \right]^{-1} \quad (3)$$

is the s -wave scattering amplitude renormalized by the long-range Coulomb interaction, with $h(\lambda) = \lambda^2 \sum_{n=1}^{\infty} [n(n^2 + \lambda^2)]^{-1} - C - \ln[\lambda]$ where $C = 0.5772$ is the Euler constant. $K_c(k^*) = \frac{1}{f_0} + \frac{1}{2} d_0 k^{*2} + P k^{*4} + \dots$ is the effective range function, where d_0 is the effective radius of the strong interaction, f_0 is the scattering length, and P is the shape parameter. The parameters of the effective range function are important parameters characterizing the essential properties of the FSI. The discrepancy for different particle pairs can also influence the effect of FSI on source size.

The details on the formalism of the two-particle momentum correlation function can be also found in Refs. [40,44].

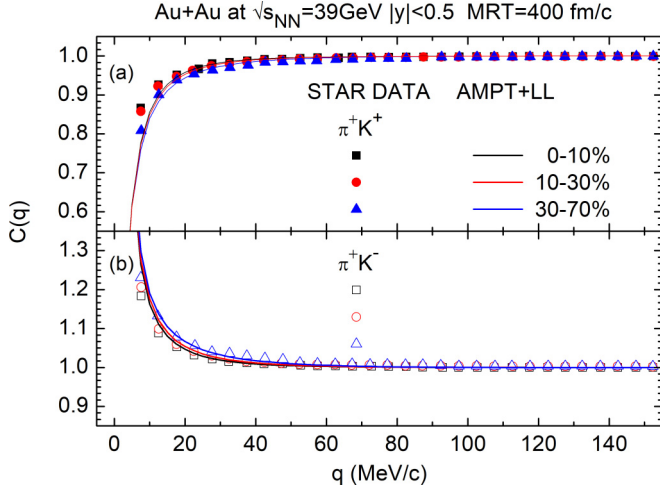


FIG. 1. Momentum correlation functions for (a) like-sign and (b) unlike-sign $\pi - K$ pairs for Au+Au collisions at $\sqrt{s_{NN}} = 39$ GeV in different centrality classes (0–10%, 10–30%, and 30–70%). Solid markers represent the preliminary experimental data from the RHIC-STAR collaboration [77,78]. Lines represent theoretical fits calculated by the AMPT model plus the Lednický and Lyuboshitz code. Note that the longer hadronic rescattering time of 400 fm/c for this meson-meson pair is used in this specific calculation for comparing with the data.

III. ANALYSIS AND DISCUSSION

A. Comparison of correlation functions between like-sign and unlike-sign particle pairs with experimental data

Figure 1 presents results of $\pi^+ - K^+$ [Fig. 1(a)] and $\pi^+ - K^-$ [Fig. 1(b)] correlation functions for three different centrality classes of 0–10%, 10–30%, and 30–70% calculated by the AMPT model combined with Lednický and Lyuboshitz code in Au + Au collisions at $\sqrt{s_{NN}} = 39$ GeV. Within the cut of transverse momentum p_t and rapidity y , we confront the experimental data with the predictions of the above analysis method. When the phase-space information of mesons with the maximum rescattering time (MRT) of 400 fm/c is selected from the AMPT model, it is found that the results can well describe the experimental data for like-sign (unlike-sign) $\pi - K$ momentum correlation functions from the RHIC-STAR Collaboration [77,78]. We can also observe a slight centrality dependence of momentum correlation function for meson pairs. Through the same conditions and calculations as Fig. 1, it is found that the results of Fig. 2 can also well describe the experimental data for the momentum correlation functions of like-sign (unlike-sign) $K - p$, $\pi - K$, $\pi - p$ from the RHIC-STAR Collaboration [77,78]. In this case, we fixed the MRT at 700 fm/c for pairs of particles containing proton [44], which could be a reasonable choice for making quantitative comparison with experimental data. However, the quantitative reproduction is not our main concern in the present work. We have checked some results for $K - p$, $\pi - K$, $\pi - p$ correlations with different MRT, such as 100 fm/c, 400 fm/c, and 700 fm/c, and find that the momentum correlations of above particles are insensitive to MRT, thus the MRT = 100 fm/c is basically a safe choice in the present work. Similar procedure

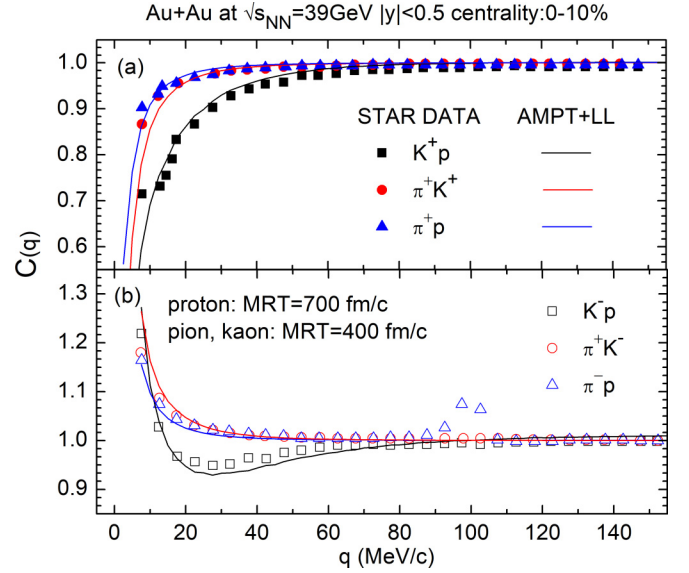


FIG. 2. Momentum correlation functions for (a) like-sign and (b) unlike-sign for kaon-proton, pion-kaon, and pion-proton pairs for central (0–10%) Au + Au collisions at $\sqrt{s_{NN}} = 39$ GeV. Solid markers represent the preliminary experimental data from the RHIC-STAR Collaboration [77,78]. Lines represent theoretical fits calculated using the AMPT model plus the Lednický and Lyuboshitz code. Note that the longer hadronic rescattering time of 400 fm/c for meson-meson pairs and 700 fm/c for proton-meson pair are used in this specific calculation for comparing with the data.

for light nuclei correlation has been performed in our previous work for the same systems at $\sqrt{s_{NN}} = 39$ GeV [44]. In order to ensure the statistics to reduce the error, we fixed the MRT at 100 fm/c in the following calculations.

B. Centrality, system-size, and P_{tot} dependence of like-sign identical meson pairs momentum correlation functions

We now perform the systematic analysis on correlation function for like-sign identical meson pairs. The $\pi^+ - \pi^+$ and $K^+ - K^+$ correlation functions will be discussed with specific gates on centrality and system size. Figures 3(a) and 3(c) present the momentum correlation functions of identical meson pairs for $^{197}_{79}\text{Au} + ^{197}_{79}\text{Au}$ collisions at different centralities of 0–10%, 10–20%, 20–40%, 40–60%, and 60–80% at $\sqrt{s_{NN}} = 39$ GeV. The momentum correlation functions of identical meson pairs exhibit more than unity in Fig. 3, which is caused by the interplay between the quantum statistical (QS) and final state interactions (FSI), and the shape is consistent with previous results [31,79,80]. The enhanced strength of the $\pi^+ - \pi^+$ and $K^+ - K^+$ momentum correlation functions is observed in peripheral collisions. These results indicate that meson emission occurs from a source with smaller space extent in peripheral collision. In addition, the effect of system size on the momentum correlation functions of mesons is also investigated by four different systems, namely $^{10}_5\text{B} + ^{10}_5\text{B}$, $^{16}_8\text{O} + ^{16}_8\text{O}$, $^{40}_{20}\text{Ca} + ^{40}_{20}\text{Ca}$, and $^{197}_{79}\text{Au} + ^{197}_{79}\text{Au}$ in central collisions. In Figs. 3(b) and 3(d), the $\pi^+ - \pi^+$ and $K^+ - K^+$ momentum correlation functions appear strong sensitivity to system size and an enhanced strength is observed when

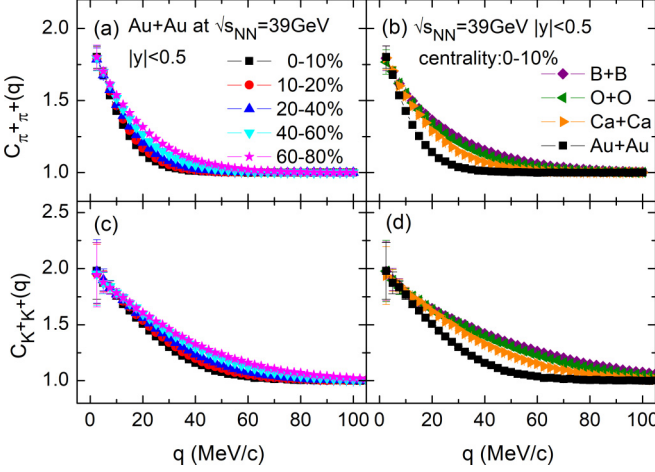


FIG. 3. Momentum correlation functions at midrapidity ($|y| < 0.5$) of pion pairs and kaon pairs as a function of five different centralities for $^{197}\text{Au} + ^{197}\text{Au}$ collisions at $\sqrt{s_{NN}} = 39$ GeV are presented in (a) and (c), respectively. Momentum correlation functions of pion pairs and kaon pairs at midrapidity ($|y| < 0.5$) for 0–10% central collisions of $^{10}_5\text{B} + ^{10}_5\text{B}$, $^{16}_8\text{O} + ^{16}_8\text{O}$, $^{40}_{20}\text{Ca} + ^{40}_{20}\text{Ca}$ as well as $^{197}_{79}\text{Au} + ^{197}_{79}\text{Au}$ systems at $\sqrt{s_{NN}} = 39$ GeV are presented in (b) and (d), respectively.

meson pairs are emitted from smaller system collisions. This enhanced strength of the momentum correlation functions for meson pairs is a physical effect stemming from the smaller space extent of the emission source [8]. Therefore, the emission source size of meson pairs obtained by their momentum correlation functions and system size is self-consistent.

In order to observe directly the contributions from centrality and system size on the two-particle correlations, then the Gaussian source radius is extracted by assuming a Gaussian-type emission source, i.e., $S(\mathbf{r}^*) \approx \exp(-\mathbf{r}^{*2}/(4r_0^2))$, where r_0 is the Gaussian source radius from the correlation functions. Figure 4 shows the P_{tot} ($P_{\text{tot}} = \mathbf{p}_1 + \mathbf{p}_2$) dependence of the Gaussian source radius of the two-meson momentum correlation functions for different centrality and system-size by the AMPT model. Figures 4(a) and 4(c) present the HBT radius of the two-meson for $^{197}\text{Au} + ^{197}\text{Au}$ collisions at different centralities of 0–10%, 10–20%, 20–40%, 40–60%, and 60–80% at $\sqrt{s_{NN}} = 39$ GeV. It is seen from Fig. 4 that the radius decreases with the increasing of transverse momentum. The trend of these results is consistent with those from theory and the STAR experiment for the same system [31,80]. Qualitatively speaking, high transverse momentum mesons are ejected from the emission source earlier, while the low transverse momentum meson emits later; therefore, we can see the expansion of the emission source by the P_{tot} dependence of the radii. It does not conflict with the understanding via radial flow effect [80,81], namely the particles with higher p_t may decouple earlier than those with lower p_t from the fireball. Meanwhile, the P_{tot} dependence of the radius of the two-meson momentum correlation functions appear slight sensitivity to centrality and system size in Fig. 4. However, the sensitivity seems to disappear in the small systems as shown in Figs. 4(b) and 4(d). In addition, the P_{tot} dependence of the

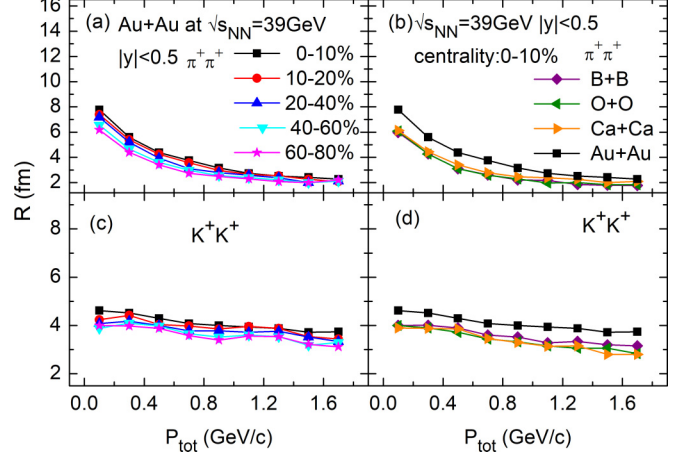


FIG. 4. P_{tot} dependence of the HBT radii at midrapidity ($|y| < 0.5$) of pion pairs and kaon pairs as a function of five different centralities for $^{197}\text{Au} + ^{197}\text{Au}$ collisions at $\sqrt{s_{NN}} = 39$ GeV are presented in (a) and (c), respectively. P_{tot} dependence of the HBT radii of pion pairs and kaon pairs at midrapidity ($|y| < 0.5$) for 0–10% central collisions of $^{10}_5\text{B} + ^{10}_5\text{B}$, $^{16}_8\text{O} + ^{16}_8\text{O}$, $^{40}_{20}\text{Ca} + ^{40}_{20}\text{Ca}$ as well as $^{197}_{79}\text{Au} + ^{197}_{79}\text{Au}$ systems at $\sqrt{s_{NN}} = 39$ GeV are presented in (b) and (d), respectively.

radius for the $\pi^+ - \pi^+$ appears more sensitive to centrality and system size than the one for $K^+ - K^+$.

C. Momentum correlation functions for like-sign (unlike-sign) nonidentical particles gated on centrality and system size

Now we investigate centrality and system-size dependence of the like-sign (unlike-sign) nonidentical particle momentum correlation functions, such as $K^+ - p$, $K^- - p$, $\pi^+ - p$, $\pi^- - p$, $\pi^+ - K^+$, and $\pi^+ - K^-$. Figures 5(a) and 5(c) show

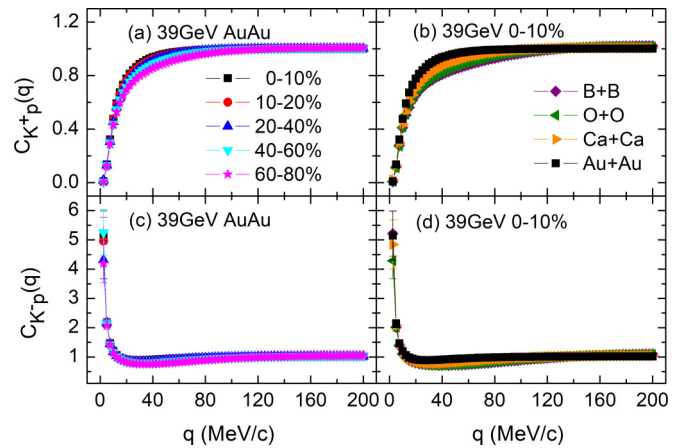


FIG. 5. Momentum correlation functions at midrapidity ($|y| < 0.5$) of like-sign (unlike-sign) kaon proton as a function of five different centralities for $^{197}\text{Au} + ^{197}\text{Au}$ collisions at $\sqrt{s_{NN}} = 39$ GeV are presented in (a) and (c), respectively. Momentum correlation functions of like-sign (unlike-sign) kaon proton at midrapidity ($|y| < 0.5$) for 0–10% central collisions of $^{10}_5\text{B} + ^{10}_5\text{B}$, $^{16}_8\text{O} + ^{16}_8\text{O}$, $^{40}_{20}\text{Ca} + ^{40}_{20}\text{Ca}$ as well as $^{197}_{79}\text{Au} + ^{197}_{79}\text{Au}$ systems at $\sqrt{s_{NN}} = 39$ GeV are presented in (b) and (d), respectively.

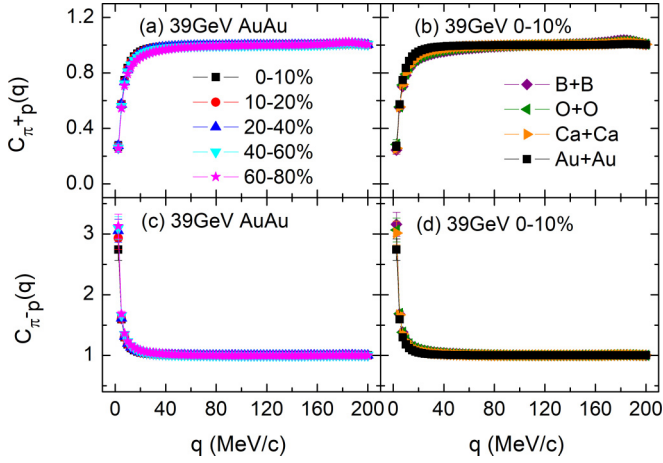


FIG. 6. Same as Fig. 5 but for pion proton.

results for the momentum correlation functions of $K^+ - p$ and $K^- - p$ for the same centrality classes as Fig. 3. The same centrality dependence is also clearly seen in Fig. 5(a). In addition, Figs. 5(b) and 5(d) show system-size dependence of $K^+ - p$ and $K^- - p$ momentum correlation functions.

We observe an enhanced strength of momentum correlation function for particle pairs in smaller systems in Fig. 5(b). However, centrality and system-size dependence of the unlike-sign particle momentum correlation functions are almost disappeared in Figs. 5(c) and 5(d). In the same way, we also investigate the effects of different centralities and system size on the momentum correlation functions of $\pi^+ - p$, $\pi^- - p$, $\pi^+ - K^+$, and $\pi^+ - K^-$ in Figs. 6 and 7. The results are similar to those in Fig. 5. In Figs. 6(b) and 7(b), system-size dependence of the $\pi^+ - p$ and $\pi^+ - K^+$ momentum correlation functions appears more sensitive to system size only in the large system such as Au and Ca.

Figure 8 shows the dependence of radius extracted from like-sign nonidentical particle momentum correlation functions gated on centrality and system size, where the squares, circles, and triangles are results for $K^+ - p$, $\pi^+ - K^+$, and $\pi^+ - p$, respectively. It is seen that the larger centrality leads

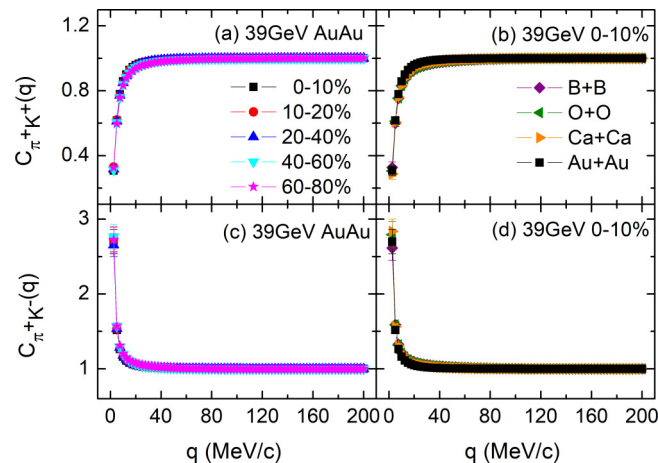


FIG. 7. Same as Fig. 5 but for pion kaon.

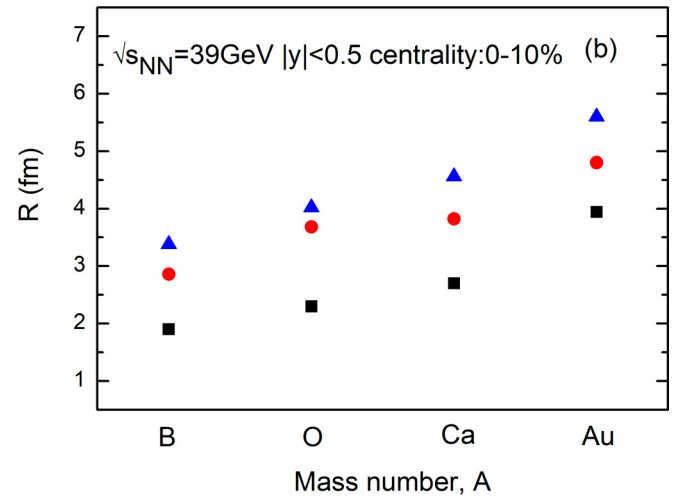
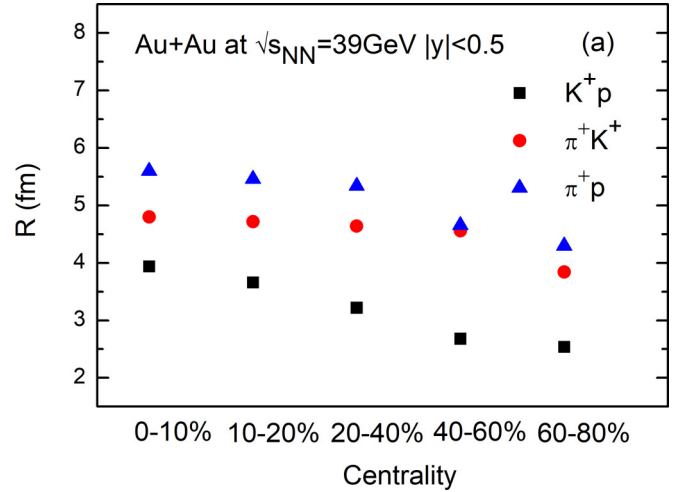


FIG. 8. (a) Centrality dependence of kaon-proton, pion-kaon, and pion-proton source size (R) for Au+Au collisions at $\sqrt{s_{NN}} = 39$ GeV. (b) System size dependence of kaon-proton, pion-kaon, and pion-proton source size (R) for 0–10% central collisions of $^{10}\text{B} + ^{10}\text{B}$, $^{16}\text{O} + ^{16}\text{O}$, $^{40}\text{Ca} + ^{40}\text{Ca}$ as well as $^{197}\text{Au} + ^{197}\text{Au}$ systems at $\sqrt{s_{NN}} = 39$ GeV.

to the smaller radius as shown in Fig. 8(a). For system-size dependence of the radii, we find that the radii generally increase with system size in Fig. 8(b). Meanwhile, the source radii from $K^+ - p$ correlation functions are smaller than those extracted from $\pi^+ - p$, $\pi^+ - K^+$ in Fig. 8, which comes from stronger correlation, i.e., the smaller Bohr radius [82–84]. The results are similar to the previous results [77,78]. In an alternative viewpoint from freezeout, the smaller R of $K^+ - p$ source indicates earlier freezeout of p and/or K^+ rather than π^+ and/or K , which has larger R of $K^+ - \pi$. Later in this paper, we find that the emission order of p , K , and π is consistent with the extracted source size.

D. Velocity selected momentum correlation functions for like-sign nonidentical particles

Momentum correlation functions of unlike particles can provide an independent constrain on their mean emission

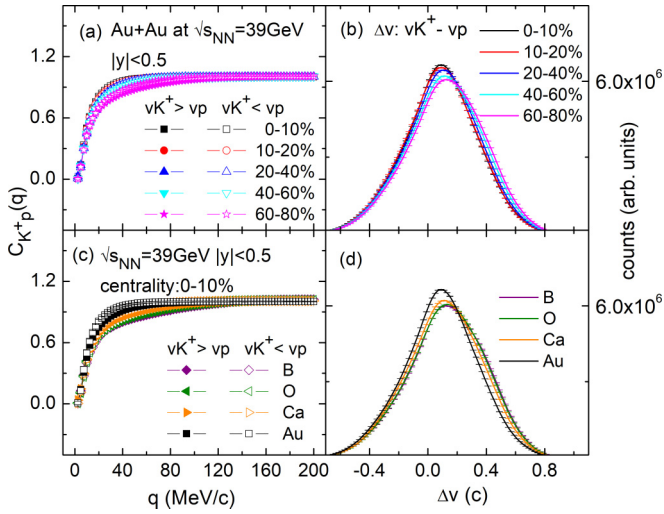


FIG. 9. Centrality and system dependence of kaon-proton (like-sign) velocity-gated momentum correlation functions and velocity difference (Δv) by the AMPT + LL model. The velocity conditions are indicated in each panel: $\Delta v > 0$ is remarked by solid symbol and the $\Delta v < 0$ by open symbol.

order by simply making velocity selections [15,39,45,85,86]. The physics details can be seen in the literature [44], which has been well applied to explore the light (anti)nuclei momentum correlation functions. Figures 9–11 present the velocity-gated momentum correlation functions as well as velocity difference (Δv) spectra of like-sign unlike particles pairs $K^+ - p$, $\pi^+ - p$, and $\pi^+ - K^+$ for 39 GeV $^{197}\text{Au} + ^{197}\text{Au}$ collisions at different centralities of 0–10%, 10–20%, 20–40%, 40–60%, and 60–80%, respectively.

Figures 9–11, panels (a), (b), show centrality dependence of velocity-gated momentum correlation functions and velocity difference (Δv) spectra of $K^+ - p$, $\pi^+ - p$, and $\pi^+ - K^+$ pairs, respectively. For $K^+ - p$ and $\pi^+ - p$ pairs, the momentum correlation functions with $v_{K^+} > v_p$ ($v_{\pi^+} > v_p$) are stronger than the ones with the reverse situation $v_{K^+} < v_p$

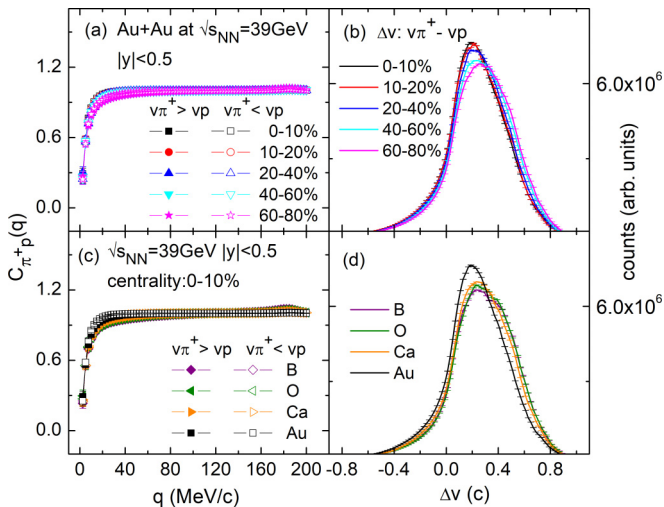


FIG. 10. Same as Fig. 9 but for pion proton.

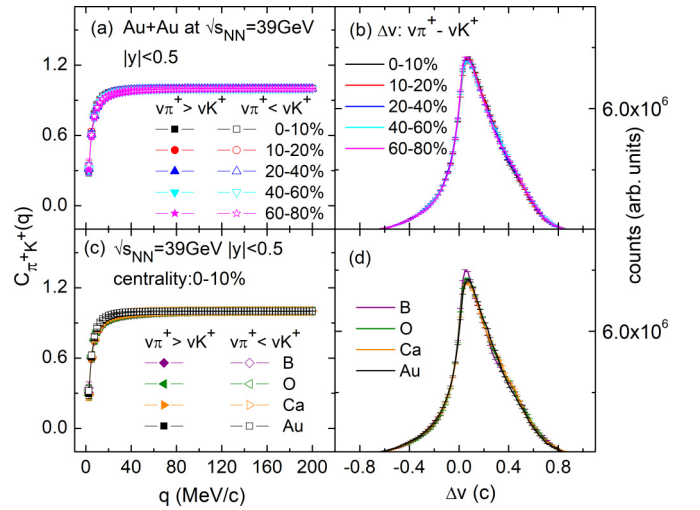


FIG. 11. Same as Fig. 9 but for pion kaon.

($v_{\pi^+} < v_p$) in Figs. 9(a) and 10(a). The comparison of two velocity-gated correlation strengths gives that the mean order of emission of protons are emitted averagely earlier than π^+ and K^+ according to the criteria [44]. The similar trend for $\pi^+ - K^+$ pairs is not so obvious overall in Fig. 11(a).

Meanwhile, Figs. 9(b), 10(b), and 11(b) present velocity difference spectra for $K^+ - p$, $\pi^+ - p$, and $\pi^+ - K^+$ pairs, respectively. The velocity difference spectra are all asymmetric due to the mean emission order. In addition, an enhanced difference between the momentum correlation functions for $K^+ - p$ ($\pi^+ - p$ or $\pi^+ - K^+$) pairs with $v_p > v_{K^+}$ ($v_p > v_{\pi^+}$ or $v_{\pi^+} > v_{K^+}$) and ones on the reverse situation at larger centrality, which manifests larger interval of the mean emission order for unlike particles in peripheral collisions.

Their ratios shown in Figs. 12(a), 13(a), and 14(a) also illustrate the above phenomenon. The system-size dependence for $K^+ - p$, $\pi^+ - p$, and $\pi^+ - K^+$ pairs is found by the fact that momentum correlation functions with $v_{K^+} > v_p$ ($v_{\pi^+} > v_p$) are stronger than the ones with the reverse situation $v_{K^+} < v_p$ ($v_{\pi^+} < v_p$) in Figs. 9(c), 10(c), and 11(c). Correspondingly, the velocity difference spectra for $K^+ - p$, $\pi^+ - p$, and $\pi^+ - K^+$ pairs are all asymmetric about $\Delta v = 0$ caused by the average emission order in Figs. 9(d), 10(d), and 11(d). All the correlation ratios for the pairs of $K^+ - p$, $\pi^+ - p$, and $\pi^+ - K^+$ generally demonstrate a dip below 1 in Figs. 12(a), 13(a), and 14(a), which indicate that the emission order is, respectively, $\tau_{K^+} > \tau_p$, $\tau_{\pi^+} > \tau_p$, and $\tau_{\pi^+} > \tau_{K^+}$. Then we can get $\tau_p < \tau_{K^+} < \tau_{\pi^+}$, i.e., the proton is on average emitted earliest, then K^+ is in the middle, and π^+ is the latest. This conclusion seems to be consistent with the different freezeout time for π , K , and p in a blast wave model analysis [87], where the freezeout temperature increases with the particle's mass (π , K , and proton), but the kinetic freezeout volume decreases with the increase of particle mass, i.e., it indicates a mass-dependent differential kinetic freezeout scenario. As mentioned above, the source size extracted from different meson-baryon or meson-meson pairs in this work (Fig. 8) is generally consistent with the mass-dependent kinetic freezeout volume. However, the emission

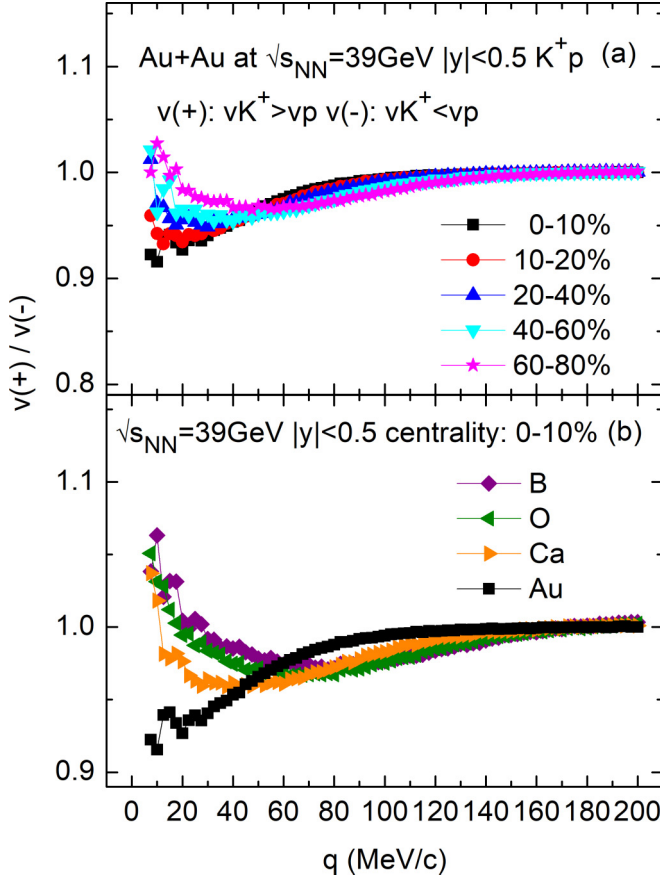


FIG. 12. (a) Ratios of the velocity-gated momentum correlation functions of kaon-proton for 39 GeV $^{197}_{79}\text{Au} + ^{197}_{79}\text{Au}$ collision at midrapidity ($|y| < 0.5$) and five different centralities. (b) Ratios of the velocity-gated momentum correlation functions of kaon proton for 0–10 % central collisions of $^{10}_5\text{B} + ^{10}_5\text{B}$, $^{16}_8\text{O} + ^{16}_8\text{O}$, $^{40}_{20}\text{Ca} + ^{40}_{20}\text{Ca}$ as well as $^{197}_{79}\text{Au} + ^{197}_{79}\text{Au}$ systems at $\sqrt{s_{\text{NN}}} = 39$ GeV.

chronology among π , K , and p looks like a reverse mass dependent in comparison with the emission order for light nuclei, such as p , d , and t as investigated in Ref. [44], in which the heavier species are emitted later in the small relative momentum region due to the nucleonic coalescence picture.

In addition, the system-size dependence of velocity-gated momentum correlation functions is also generally observed by their ratios in Figs. 12(b), 13(b), and 14(b). With the decreasing of system size, we observe an enhanced difference between the momentum correlation functions for $K^+ - p$ ($\pi^+ - p$ or $\pi^+ - K^+$) pair with $v_p > v_{K^+}$ ($v_p > v_{\pi^+}$ or $v_{\pi^+} > v_{K^+}$) and the ones with the reverse situation in Figs. 9(c), 10(c), and 11(c). The dependence on system size for the momentum correlation functions of meson-baryon or meson-meson particle pairs is caused by the emission source of different particles as shown in Fig. 8(b). In the viewpoint of emission order, we can generally say that the emission duration among p , K and π could be larger for the smaller system than the larger system, especially for π -hadron correlations (Figs. 13 and 14). For $K^+ - p$ combination (Fig. 12), it is noted that the ratio shows first drop to a dip, then rises for light collision systems, which is different from the case of Au + Au

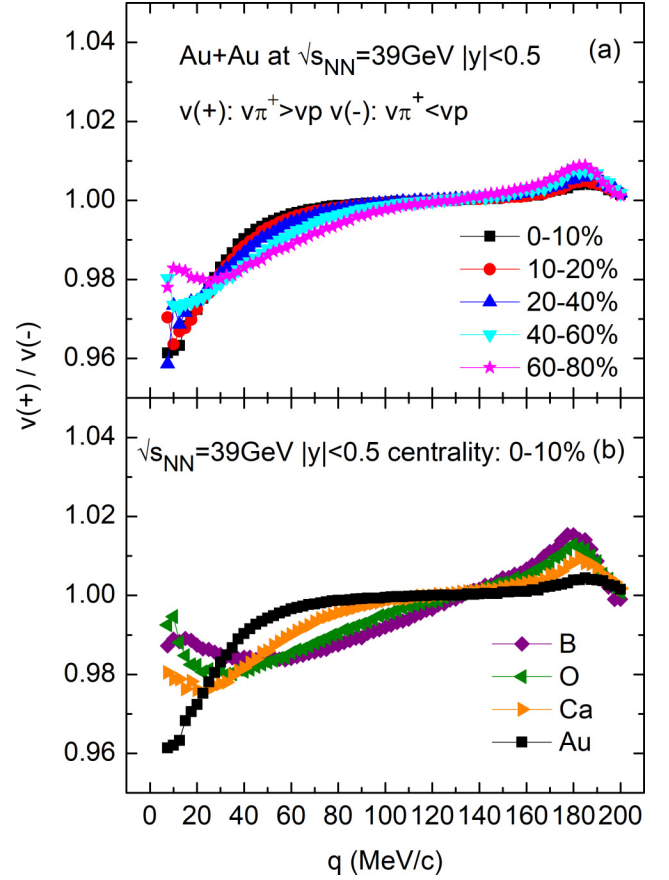


FIG. 13. Same as Fig. 12 but for pion proton.

collision. In particular, the ratios display the values above 1 in the lowest relative momentum, which illustrates that $\tau_p > \tau_{K^+}$, i.e., proton is emitted on average later than K^+ . At around $q \approx 20$ MeV/c, the ratios display the values below 1, i.e., $\tau_p < \tau_{K^+}$, then $\tau_p \simeq \tau_{K^+}$ at larger q . However, the fine structure for each ratios of meson-meson and meson-baryon correlations demonstrates slight differences, which indicates slightly different emission chronology.

IV. SUMMARY

In summary, with the AMPT model complemented by the Lednický and Lyuboshitz analytical method, we have constructed and analyzed the momentum correlation functions of like-sign (unlike-sign) particle for heavy-ion collisions with different system sizes and centralities for $\sqrt{s_{\text{NN}}} = 39$ GeV Au + Au collisions. We present a comparison of like-sign (unlike-sign) $K - p$, $\pi - K$, and $\pi - p$ momentum correlation functions with the experimental data from the RHIC-STAR Collaboration [77,78]. Taking the same transverse momentum and rapidity phase space coverage corresponding to the experimental situation as well as the maximum hadronic rescattering time selected by mesons of 400 fm/c and proton of 700 fm/c in AMPT, it is found that the like-sign (unlike-sign) $K - p$, $\pi - K$, and $\pi - p$ momentum correlation functions simulated by the present model can match the experimental data. We further study centrality

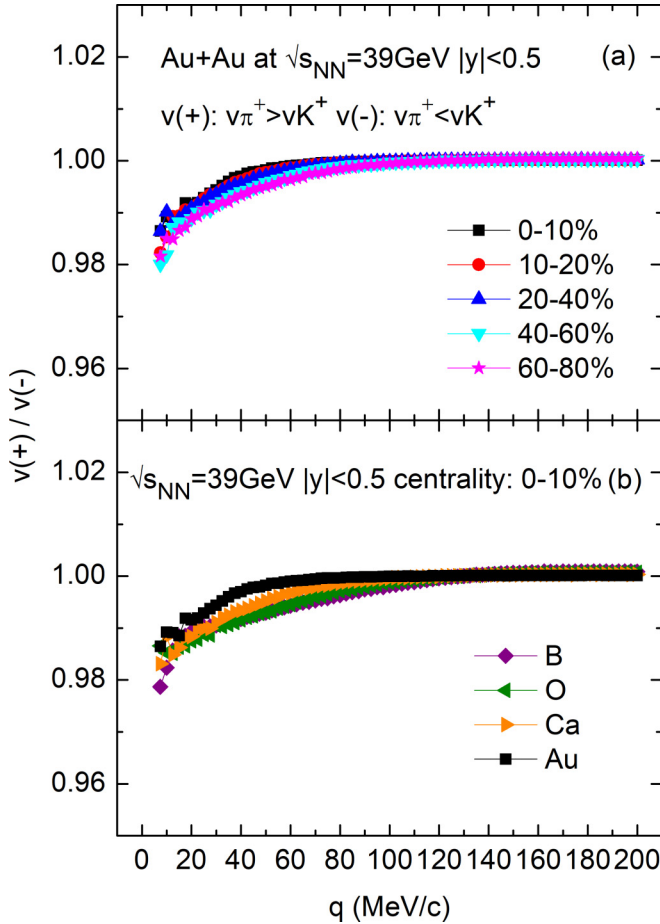


FIG. 14. Same as Fig. 12 but for pion kaon.

and system-size dependence of momentum correlation functions for identical and nonidentical particle pairs, respectively,

which is in the condition of the maximum hadronic rescattering time of 100 fm/c in AMPT. The shape of momentum correlation functions for particle pairs is consistent with previous works [31,79,80], which is caused by both QS and FSI.

The centrality dependence of momentum correlation functions for particles is investigated by $^{197}\text{Au} + ^{197}\text{Au}$ collisions at five centralities of 0–10%, 10–20%, 20–40%, 40–60%, and 60–80% at $\sqrt{s_{NN}} = 39$ GeV. It is found that with increasing centralities from center to periphery, the momentum correlation functions for particles become stronger, which is consistent with the emission from the smaller source. The momentum correlation functions of particles are sensitive to system size through studying $^{10}\text{B} + ^{10}\text{B}$, $^{16}\text{O} + ^{16}\text{O}$, $^{40}\text{Ca} + ^{40}\text{Ca}$, and $^{197}\text{Au} + ^{197}\text{Au}$ in central collisions, and used to obtain the emission source size of particles, which is self-consistent with their system size. Furthermore, momentum correlation functions between nonidentical particles shed light on important information about the average emission sequence of them. Through the correlation functions gated with the velocity, it is deduced that protons are generally emitted earliest, K is in middle, and π is the latest in the small relative momentum region, which indicates mass-dependent kinetic freezeout scenario. Experimental analysis along this direction is expected.

ACKNOWLEDGMENTS

This work was supported in part by the National Natural Science Foundation of China under Contracts No. 11890710, No. 11890714, No. 11875066, No. 11925502, No. 11961141003, No. 11935001, No. 12147101, and No. 12047514, the Strategic Priority Research Program of CAS under Grant No. XDB34000000, National Key R&D Program of China under Grants No. 2018YFE0104600 and No. 2016YFE0100900, Guangdong Major Project of Basic and Applied Basic Research No. 2020B0301030008.

- [1] R. H. Brown and R. Q. Twiss, Correlation between photons in two coherent beams of light, *Nature (London)* **177**, 27 (1956).
- [2] R. H. Brown and R. Q. Twiss, A test of a new type of stellar interferometer on sirius, *Nature (London)* **178**, 1046 (1956).
- [3] S. E. Koonin, Proton pictures of high-energy nuclear collisions, *Phys. Lett. B* **70**, 43 (1977).
- [4] M. A. Lisa, S. Pratt, R. Soltz, and U. Wiedemann, Femtoscopy in relativistic heavy ion collisions: Two decades of progress, *Annu. Rev. Nucl. Part. Sci.* **55**, 357 (2005).
- [5] U. A. Wiedemann and U. Heinz, Particle interferometry for relativistic heavy-ion collisions, *Phys. Rep.* **319**, 145 (1999).
- [6] G. Goldhaber, S. Goldhaber, W. Lee, and A. Pais, Influence of bose-einstein statistics on the antiproton-proton annihilation process, *Phys. Rev.* **120**, 300 (1960).
- [7] A. Bialas, M. Kucharczyk, H. Palka, and K. Zalewski, Mass dependence of hbt correlations in e^+e^- annihilation, *Phys. Rev. D* **62**, 114007 (2000).
- [8] R. Ghatti *et al.*, Characterization of nuclear sources from neutron-neutron, proton-proton and neutron-proton correlation functions, *Nucl. Phys. A* **674**, 277 (2000).
- [9] D. H. Boal, C. K. Gelbke, and B. K. Jennings, Intensity interferometry in subatomic physics, *Rev. Mod. Phys.* **62**, 553 (1990).
- [10] D. Ardouin, Recent light particle correlation data from heavy ion collisions at intermediate and low energies, *Int. J. Mod. Phys. E* **06**, 391 (1997).
- [11] R. Ghatti, J. Helgesson, V. Avdeichikov *et al.*, Chronology of particle emission from the $e/a = 61$ MeV $^{36}\text{Ar} + ^{27}\text{Al}$ reaction, *Phys. Rev. Lett.* **91**, 092701 (2003).
- [12] J. J. He, S. Zhang, Y. G. Ma, J. H. Chen, and C. Zhong, Clustering structure effect on hanbury-brown-twiss correlation in $^{12}\text{C} + ^{197}\text{Au}$ collisions at 200 GeV, *Eur. Phys. J. A* **56**, 52 (2020).
- [13] T. T. Wang, Y. G. Ma, C. J. Zhang, and Z. Q. Zhang, Effect of in-medium nucleon-nucleon cross section on proton-proton momentum correlation in intermediate-energy heavy-ion collisions, *Phys. Rev. C* **97**, 034617 (2018).
- [14] R. Kotte *et al.*, Two-proton small-angle correlations in central heavy-ion collisions: A beam-energy- and system-size-dependent study, *Eur. Phys. J. A* **23**, 271 (2005).

- [15] D. Gourio *et al.*, Emission time scale of light particles in the system Xe + Sn at 50 AMeV. A probe for dynamical emission? *Eur. Phys. J. A* **7**, 245 (2000).
- [16] J. Pochodzalla, C. K. Gelbke, W. G. Lynch *et al.*, Two-particle correlations at small relative momenta for ^{40}Ar induced reactions on ^{197}Au at $E/A = 60\text{MeV}$, *Phys. Rev. C* **35**, 1695 (1987).
- [17] W. G. Gong, W. Bauer, C. K. Gelbke, and S. Pratt, Space-time evolution of nuclear reactions probed by two-proton intensity interferometry, *Phys. Rev. C* **43**, 781 (1991).
- [18] Y. G. Ma, Y. B. Wei, W. Q. Shen *et al.*, Surveying the nucleon-nucleon momentum correlation function in the framework of quantum molecular dynamics model, *Phys. Rev. C* **73**, 014604 (2006).
- [19] R. Gheiti, V. Avdeichikov, B. Jakobsson, P. Golubev, J. Helgesson, N. Colonna, G. Tagliente, H. W. Wilschut, S. Kopecky, V.L. Kravchuk, E. W. Anderson, P. Nadel-Turonski, L. Westerberg, V. Bellini, M. L. Sperduto, and C. Sutura, Isospin effects on two-particle correlation functions in $E/A = 61\text{ MeV}$ $^{36}\text{Ar} + ^{112,124}\text{Sn}$ reactions, *Phys. Rev. C* **69**, 031605(R) (2004).
- [20] L. W. Chen, V. Greco, C. M. Ko, and B. A. Li, Effects of symmetry energy on two-nucleon correlation functions in heavy-ion collisions induced by neutron-rich nuclei, *Phys. Rev. Lett.* **90**, 162701 (2003).
- [21] D. Q. Fang, Y. G. Ma, X. Y. Sun *et al.*, Proton-proton correlations in distinguishing the two-proton emission mechanism of ^{23}Al and ^{22}Mg , *Phys. Rev. C* **94**, 044621 (2016).
- [22] B. S. Huang and Y. G. Ma, Two-proton momentum correlation from photodisintegration of α -clustering light nuclei in the quasideuteron region, *Phys. Rev. C* **101**, 034615 (2020).
- [23] L. Shen, B. S. Huang, and Y. G. Ma, Short-range correlations in the extended quantum molecular dynamics model, *Phys. Rev. C* **105**, 014603 (2022).
- [24] T. T. Wang, Y. G. Ma, D. Q. Fang, and H. L. Liu, Temperature and density effects on the two-nucleon momentum correlation function from excited single nuclei, *Phys. Rev. C* **105**, 024620 (2022).
- [25] L. M. Fang, Y. G. Ma, and S. Zhang, Azimuthal-sensitive three-dimensional hbt radius in Au+Au collisions at $E_{\text{beam}} = 1.23\text{A GeV}$ by the iqmd model, *Eur. Phys. J. A* **58**, 81 (2022).
- [26] P. Li, J. Steinheimer, T. Reichert, A. Kittiratpattana, M. Bleicher, and Q. Li, Effects of a phase transition on two-pion interferometry in heavy ion collisions at root $\sqrt{s_{NN}} = 2.4\text{--}7.7\text{ GeV}$, *Sci. China Phys. Mech. Astron.* **66**, 232011 (2023).
- [27] P. Li, Y. Wang, Q. Li, and H. Zhang, Transport model analysis of the pion interferometry in Au + Au collisions at $E_{\text{beam}} = 1.23\text{ GeV/nucleon}$, *Sci. China Phys. Mech. Astron.* **66**, 222011 (2023).
- [28] P. Scott, Constraining the high density nuclear equation of state with femtoscopic pion correlations, *Sci. China Phys. Mech. Astron.* **66**, 252032 (2023).
- [29] S. Voloshin, R. Lednický, S. Panitkin, and N. Xu, Relative space-time asymmetries in pion and nucleon production in non-central nucleus-nucleus collisions at high energies, *Phys. Rev. Lett.* **79**, 4766 (1997).
- [30] D. Ardouin, S. Soff, C. Spieles *et al.*, Unlike particle correlations and the strange quark matter distillation process, *Phys. Lett. B* **446**, 191 (1999).
- [31] Z. Q. Zhang, S. Zhang, and Y. G. Ma, Simulation of energy scan of pion interferometry in central Au+Au collisions at relativistic energies, *Chin. Phys. C* **38**, 014102 (2014).
- [32] J. Adams *et al.* (STAR Collaboration), Azimuthally sensitive Hanbury Brown – Twiss Interferometry in Au + Au collisions at $\sqrt{s_{NN}} = 200\text{ GeV}$, *Phys. Rev. Lett.* **93**, 012301 (2004).
- [33] C. Adler *et al.* (STAR Collaboration), Pion interferometry of $\sqrt{s_{NN}} = 130\text{ GeV}$ Au + Au collisions at rhic, *Phys. Rev. Lett.* **87**, 082301 (2001).
- [34] L. Adamczyk *et al.* (STAR Collaboration), Measurement of interaction between antiprotons, *Nature (London)* **527**, 345 (2015).
- [35] L. Adamczyk *et al.* (STAR Collaboration), $\Lambda\Lambda$ correlation function in Au + Au collisions at $\sqrt{s_{NN}} = 200\text{ GeV}$, *Phys. Rev. Lett.* **114**, 022301 (2015).
- [36] J. Adam, L. Adamczyk *et al.* (STAR Collaboration), The proton- ω correlation function in Au + Au collisions at $\sqrt{s_{NN}} = 200\text{ GeV}$, *Phys. Lett. B* **790**, 490 (2019).
- [37] S. Acharya *et al.* (ALICE Collaboration), Unveiling the strong interaction among hadrons at the LHC, *Nature (London)* **588**, 232 (2020).
- [38] S. Acharya *et al.* (ALICE Collaboration), Towards the understanding of the genuine three-body interaction for $p - p - p$ and $p - p - \Lambda$, *Eur. Phys. J. A* **59**, 145 (2023).
- [39] R. Lednický, V. Lyuboshitz, B. Erazmus, and D. Nouais, How to measure which sort of particles was emitted earlier and which later, *Phys. Lett. B* **373**, 30 (1996).
- [40] T. T. Wang, Y. G. Ma, and Z. Q. Zhang, Effects of P_{tot} gates and velocity gates on light-particle momentum correlation in intermediate-energy heavy-ion collisions, *Phys. Rev. C* **99**, 054626 (2019).
- [41] Y. J. Wang, F. H. Guan, Q. H. Wu *et al.*, The emission order of hydrogen isotopes via correlation functions in 30 MeV/u Ar + Au reactions, *Phys. Lett. B* **825**, 136856 (2022).
- [42] B. S. Xi, Z. Q. Zhang, S. Zhang, and Y. G. Ma, Searching for ^4Li via the momentum-correlation function of $\bar{p}\text{--}^3\text{He}$, *Phys. Rev. C* **102**, 064901 (2020).
- [43] R. Kotte *et al.*, On the space-time difference of proton and composite particle emission in central heavy-ion reactions at 400 AMeV, *Eur. J. Phys. A* **6**, 185 (1999).
- [44] T. T. Wang, Y. G. Ma, and S. Zhang, Simulations of momentum correlation functions of light (anti)nuclei in relativistic heavy-ion collisions at $\sqrt{s_{NN}} = 39\text{ GeV}$, *Phys. Rev. C* **107**, 014911 (2023).
- [45] C. Gelderloos and J. M. Alexander, A probe of emission order and time delay for pairs of ejectiles in nuclear reactions, *Nucl. Instrum. Methods Phys. Res. Sect. A* **349**, 618 (1994).
- [46] Z. W. Lin, C. M. Ko, B. A. Li, B. Zhang, and S. Pal, Multiphase transport model for relativistic heavy ion collisions, *Phys. Rev. C* **72**, 064901 (2005).
- [47] Z. W. Lin and L. Zheng, Further developments of a multi-phase transport model for relativistic nuclear collisions, *Nucl. Sci. Tech.* **32**, 113 (2021).
- [48] R. A. Lacey, Indications for a critical end point in the phase diagram for hot and dense nuclear matter, *Phys. Rev. Lett.* **114**, 142301 (2015).
- [49] M. I. Abdulhamid *et al.* (STAR Collaboration), Beam energy dependence of triton production and yield ratio ($N_t \times N_p / N_d^2$) in Au + Au collisions at RHIC, *Phys. Rev. Lett.* **130**, 202301 (2023).

- [50] J. L. Nagle and W. A. Zajc, Small system collectivity in relativistic hadronic and nuclear collisions, *Annu. Rev. Nucl. Part. Sci.* **68**, 211 (2018).
- [51] S. Zhang, Y. G. Ma, G. L. Ma, J. H. Chen, Q. Y. Shou, W. B. He, and C. Zhong, Collision system size scan of collective flows in relativistic heavy-ion collisions, *Phys. Lett. B* **804**, 135366 (2020).
- [52] S. Huang, Z. Chen, W. Li, and J. Jia, Disentangling contributions to small-system collectivity via scans of light nucleus-nucleus collisions, *Phys. Rev. C* **101**, 021901(R) (2020).
- [53] Z. Citron, A. Dainese, J. Grosse-Oetringhaus *et al.*, [arXiv:1812.06772](https://arxiv.org/abs/1812.06772).
- [54] Y.-Z. Wang, S. Zhang, and Y.-G. Ma, System dependence of away-side broadening and α -clustering light nuclei structure effect in dihadron azimuthal correlations, *Phys. Lett. B* **831**, 137198 (2022).
- [55] Star review talk, Quark Matter 2023, <https://indico.cern.ch/event/1139644/>.
- [56] R. Lednický, Femtoscopic correlations in multiparticle production and beta-decay, *Braz. J. Phys.* **37**, 939 (2007).
- [57] R. Lednický, Correlation femtoscopy, *Nucl. Phys. A* **774**, 189 (2006).
- [58] R. Lednický, Finite-size effect on two-particle production in continuous and discrete spectrum, *Phys. Part. Nuclei* **40**, 307 (2009).
- [59] R. Lednický, Notes on correlation femtoscopy, *Phys. Atom. Nuclei* **71**, 1572 (2008).
- [60] S. Zhang, J. H. Chen, H. Crawford, D. Keane, Y. G. Ma, and Z. B. Xu, Searching for onset of deconfinement via hypernuclei and baryon-strangeness correlations, *Phys. Lett. B* **684**, 224 (2010).
- [61] B. Alver and G. Roland, Collision-geometry fluctuations and triangular flow in heavy-ion collisions, *Phys. Rev. C* **81**, 054905 (2010).
- [62] G. L. Ma and X. N. Wang, Jets, mach cones, hot spots, ridges, harmonic flow, dihadron, and γ -hadron correlations in high-energy heavy-ion collisions, *Phys. Rev. Lett.* **106**, 162301 (2011).
- [63] L. X. Han, G. L. Ma, Y. G. Ma, X. Z. Cai, J. H. Chen, S. Zhang, and C. Zhong, Initial fluctuation effect on harmonic flows in high-energy heavy-ion collisions, *Phys. Rev. C* **84**, 064907 (2011).
- [64] A. Bzdak and G. L. Ma, Elliptic and triangular flow in p -Pb and peripheral Pb-Pb collisions from parton scatterings, *Phys. Rev. Lett.* **113**, 252301 (2014).
- [65] S. Zhang, Y. G. Ma, J. H. Chen, W. B. He, and C. Zhong, Nuclear cluster structure effect on elliptic and triangular flows in heavy-ion collisions, *Phys. Rev. C* **95**, 064904 (2017).
- [66] Y. L. Cheng, S. Zhang, and Y. G. Ma, Collision centrality and system size dependences of light nuclei production via dynamical coalescence mechanism, *Eur. Phys. J. A* **57**, 330 (2021).
- [67] H. Zhang, J. F. Liao, E. K. Wang, Q. Wang, and H. X. Xing, Deciphering the nature of X(3872) in heavy ion collisions, *Phys. Rev. Lett.* **126**, 012301 (2021).
- [68] H. Wang and J. H. Chen, Study on open charm hadron production and angular correlation in high-energy nuclear collisions, *Nucl. Sci. Tech.* **32**, 2 (2021).
- [69] H. Wang and J. H. Chen, Anisotropy flows in Pb-Pb collisions at LHC energies from parton scatterings with heavy quark trigger, *Nucl. Sci. Tech.* **33**, 15 (2022).
- [70] X. N. Wang and M. Gyulassy, HIJING: A Monte Carlo model for multiple jet production in pp, pA, and AA collisions, *Phys. Rev. D* **44**, 3501 (1991).
- [71] M. Gyulassy and X. N. Wang, Hijing 1.0: A monte carlo program for parton and particle production in high energy hadronic and nuclear collisions, *Comput. Phys. Commun.* **83**, 307 (1994).
- [72] B. Zhang, ZPC 1.0.1: a parton cascade for ultrarelativistic heavy ion collisions, *Comput. Phys. Commun.* **109**, 193 (1998).
- [73] Z.-W. Lin, S. Pal, C. M. Ko, B.-A. Li, and B. Zhang, Charged particle rapidity distributions at relativistic energies, *Phys. Rev. C* **64**, 011902(R) (2001).
- [74] S. Pal, C. M. Ko, and Z. W. Lin, Multistrange baryon production in relativistic heavy ion collisions, *Nucl. Phys. A* **730**, 143 (2004).
- [75] S. Pal, C. M. Ko, and Z. wei Lin, Phi meson production in relativistic heavy ion collisions, *Nucl. Phys. A* **707**, 525 (2002).
- [76] B. A. Li and C. M. Ko, Formation of superdense hadronic matter in high energy heavy-ion collisions, *Phys. Rev. C* **52**, 2037 (1995).
- [77] H. Zbroszczyk, Baryon-baryon correlations at the star experiment, *Acta Phys. Pol. B Proc. Suppl.* **12**, 205 (2019).
- [78] S. Siejka, Geometry and dynamics in heavy-ion collisions seen by the femtoscopy in the star experiment, *Nucl. Phys. A* **982**, 359 (2019).
- [79] J. Adamczewski-Musch, C. B. O. Arnold *et al.*, Identical pion intensity interferometry at $\sqrt{s_{NN}} = 2.4$ GeV, *Eur. Phys. J. A* **56**, 140 (2020).
- [80] J. Adams *et al.* (STAR Collaboration), Pion interferometry in Au + Au collisions at $\sqrt{s_{NN}} = 200$ GeV, *Phys. Rev. C* **71**, 044906 (2005).
- [81] Retière, Fabrice, Lisa, and M. Annan, Observable implications of geometrical and dynamical aspects of freeze-out in heavy ion collisions, *Phys. Rev. C* **70**, 044907 (2004).
- [82] A. Kisiel, Non-identical particle femtoscopy in models with single freeze-out, *Braz. J. Phys.* **37**, 917 (2007).
- [83] R. Lednický and V. Lyuboshitz, Effect of the final-state interaction on pairing correlations of particles with small relative momenta, *Sov. J. Nucl. Phys.* **35**, 770 (1982).
- [84] M. Gyulassy, S. K. Kauffmann, and L. W. Wilson, Pion interferometry of nuclear collisions. I. theory, *Phys. Rev. C* **20**, 2267 (1979).
- [85] C. J. Gelderloos, R. Sun, N. N. Ajitanand *et al.*, Emission times for energy selected $^1,2,3\text{H}$ ejectiles from central collisions: 1360 MeV $^{40}\text{Ar} + \text{Ag}$, *Phys. Rev. C* **52**, R2834(R) (1995).
- [86] B. S. Huang and Y. G. Ma, Emission time sequence of neutrons and protons as probes of α -clustering structure, *Chin. Phys. C* **44**, 094105 (2020).
- [87] M. Waqas, F.-H. Liu, L.-L. Li, and H. M. Alfanda, Effective (kinetic freeze-out) temperature, transverse flow velocity, and kinetic freeze-out volume in high energy collisions, *Nucl. Sci. Tech.* **31**, 109 (2020).